

Excitable Er fraction and quenching phenomena in Er-doped SiO₂ layers containing Si nanoclusters

B. Garrido, C. García, S.-Y. Seo, and P. Pellegrino

EME, Departament d'Electrònica, IN2UB, Universitat de Barcelona, Martí i Franquès 1, 08028, Barcelona, Spain

D. Navarro-Urrios, N. Daldosso, and L. Pavesi

Dipartimento di Fisica, Università di Trento, Via Sommarive 14, I-38050 Povo (Trento), Italy

F. Gourbilleau and R. Rizk

SIFCOM, UMR CNRS 6176, ENSICAEN, 6 Boulevard Maréchal Juin, 14050 CAEN, France

(Received 17 April 2007; revised manuscript received 18 July 2007; published 7 December 2007)

This paper investigates the interaction between Si nanoclusters (Si-nc) and Er in SiO₂, reports on the optical characterization and modeling of this system, and attempts to clarify its effectiveness as a gain material for optical waveguide amplifiers at 1.54 μm . Silicon-rich silicon oxide layers with an Er content of 4–6 $\times 10^{20}$ at./cm³ were deposited by reactive magnetron sputtering. The films with Si excess of 6–7 at. %, and postannealed at 900 °C showed the best Er³⁺ photoluminescence (PL) intensity and lifetime, and were used for the study. The annealing duration was varied up to 60 min to engineer the size and density of Si-nc and optimize Si-nc and Er coupling. PL investigations under resonant (488 nm) and nonresonant (476 nm) pumping show that an Er effective excitation cross section is similar to that of Si-nc ($\sim 10^{-17}$ – 10^{-16} cm²) at low pumping flux ($\sim 10^{16}$ – 10^{17} cm⁻² s⁻¹), while it drops at high flux ($> 10^{18}$ cm⁻² s⁻¹). We found a maximum fraction of excited Er of about 2% of the total Er content. This is far from the 50% needed for optical transparency and achievement of population inversion and gain. Detrimental phenomena that cause depletion of Er inversion, such as cooperative up conversion, excited-state absorption, and Auger deexcitations are modeled, and their impact in lowering the amount of excitable Er is found to be relatively small. Instead, Auger-type short-range energy transfer from Si-nc to Er is found, with a characteristic interaction length of 0.4 nm. Based on such results, numerical and analytical (Er as a quasi-two-level system) coupled rate equations have been developed to determine the optimum conditions for Er inversion. The modeling predicts that interaction is quenched for high photon flux and that only a small fraction of Er (0.2–2 %) is excitable through Si-nc. Hence, the low density of sensitizers (Si-nc) and the short range of the interaction are the explanation of the low fraction of Er coupled. Efficient ways to improve Er-doped Si-nc thin films for the realization of practical optical amplifiers are also discussed.

DOI: [10.1103/PhysRevB.76.245308](https://doi.org/10.1103/PhysRevB.76.245308)

PACS number(s): 42.70.Nq, 71.35.Gg, 78.55.Ap, 78.67.Bf

I. INTRODUCTION

Er³⁺ ions in silicate matrices have a long lived first excited state ($^4I_{13/2}$) and emit in a small range of wavelengths around 1.54 μm . These two facts make Er in silicates useful for optical fiber amplifiers because this spectral range corresponds to the minimum attenuation in silica-based optical fibers (losses of 0.2 dB/km) which are widely used for long distance optical communications. Er-doped fiber amplifiers (EDFAs) are used for the regeneration of signals in this optical domain and have set the standard for long-haul optical communications.^{1,2} Nevertheless, reducing their size and cost for integration in local area networks (LANs) presents serious difficulties. In order to get reasonable gain outputs (20–30 dB) the use of long fibers becomes mandatory, due to the moderate Er content (to avoid concentration quenching effects) and the small absorption cross section of Er ($\sim 10^{-21}$ cm²).² These effects, combined with the discrete nature of the electronic energy levels in Er ions, imply that high power and thus expensive and bulky laser diodes at 980 or 1480 nm must be used for the excitation. Although other glasses have been used as matrices and Yb as sensitizer,³ the pumping constraints have not been completely relaxed and

thus there is still the need to develop an appropriate material to produce Er-doped waveguide amplifiers (EDWAs) of small size, low cost, and compatible with Si technology. This accomplishment would allow their integration in LANs together with other silicon photonic components.

It was discovered in 1994 that Er emission is strongly enhanced by using Si nanocrystals as sensitizers in silica when codoped with Er.⁴ This material system can be obtained from standard silicon compatible processes, e.g., ion implantation of Si in SiO₂ or deposition of Si-rich silicon oxide layers (SiO_x), followed by high temperature annealing to induce Si nanocrystal formation. Si nanocrystals in SiO₂ have been extensively studied for more than a decade for the visible photo- and electroluminescence (PL,EL) originated from quantum confinement effects,^{5–10} and for the use of Si nanocrystals as nanosize charge-storing elements in flash memories.^{11,12} For materials codoped with Er, it was recently shown that amorphous Si nanoclusters (Si-nc) are as efficient sensitizers as Si nanocrystals.¹³ In such codoped systems (with either Si nanocrystals or nanoclusters as sensitizers), an increase of more than four orders of magnitude of an Er-effective excitation cross section was observed. This value turns out to be that of the Si-nc ($\sim 10^{-17}$ – 10^{-16} cm²).^{13–16}

Additionally, the broad absorption band of the Si clusters, used in this case to excite indirectly Er, should enable the use of cheap flash lamps or light-emitting diodes (LEDs) for side pumping, efficiently replacing the expensive pumping lasers. Furthermore, the increase of the refractive index produced by the Si-nc can be used to provide the index contrast necessary for waveguiding. These properties offer the possibility to fabricate a compact, Si-compatible, integrated, and cost-effective erbium-doped waveguide amplifier (EDWA), where the active layer is composed by silica codoped with Si-nc and Er.

The expectations were high, especially when some authors reported the increase of almost two orders of magnitude ($8 \times 10^{-20} \text{ cm}^2$) of the Er emission cross section at $1.54 \mu\text{m}$ in the codoped material with respect to that in pure silica ($\approx 2 \times 10^{-21} \text{ cm}^2$).¹⁴ This increase would allow the achievement of a gain as high as 7 dB/cm for Er concentrations N_{Er} as low as $1 \times 10^{19} \text{ cm}^{-3}$. In this range of concentration the ion-ion interactions that induce concentration quenching and up-conversion effects remain quite weak.^{2,17} Then another paper seemed to confirm these figures and the authors claimed to have reached in their EDWAs signal enhancements of 4 dB/cm and attainable gains of up to 7 dB/cm for Er doping of $\sim 1 \times 10^{19} \text{ cm}^{-3}$.¹⁸ The experiments were done by top pumping with a laser at 476 nm and with a flux of $\sim 4 \times 10^{18} \text{ cm}^{-2} \text{ s}^{-1}$. This relatively low flux is attainable with commercial LEDs and the same authors recently reported to have obtained signal enhancement by top pumping with an array of GaN LEDs.¹⁹

Recently, we have reported results on EDWAs fabricated with similar samples used in this work ($N_{\text{Er}} \approx 4-6 \times 10^{20} \text{ cm}^{-3}$) demonstrating that losses dominate at low pump powers, whereas a signal enhancement reaching 1.06 dB/cm is detected in strong pumping conditions ($6 \times 10^{21} \text{ cm}^{-2} \text{ s}^{-1}$, 488 nm pump).²⁰ Furthermore, insertion losses in the infrared Er absorption band allowed one to determine an Er^{3+} absorption cross section $\sigma_{\text{abs}} \approx 5 \times 10^{-21} \text{ cm}^2$, a result that has been recently confirmed by other authors.²¹ This seems to have closed the debate about the enhancement of the emission cross section if one considers that $\sigma_{\text{abs}} \approx \sigma_{\text{em}}$. Then, the gain reported in Ref. 18 remains unexplained. On the other hand, one could rely on increasing the Er concentration up to $N_{\text{Er}} = 4 \times 10^{20} \text{ cm}^{-3}$ to get those 7 dB/cm quoted above, once inverting the whole Er population. However, a signal enhancement of 1.06 dB/cm corresponds to a fraction of inverted Er ions of less than 10%. Additionally, most of them were directly excited as we pumped with the resonant 488 nm line.²⁰ Increasing furthermore the Er concentration would become problematic since, by means of imaging experiments with atomic resolution, we have demonstrated that for $N_{\text{Er}} \approx 6 \times 10^{20} \text{ cm}^{-3}$ and annealing temperatures of 1000 °C a significant part of the Er is clusterized, while for annealing at 900 °C there is no evidence of such a clustering.²² Both these latter experiments and the optical waveguide measurements reported in Ref. 20 allow one to infer that most of the Er ions are optically active after a 900 °C anneal while only a small fraction of them can be excited through the Si-nc.

Many aspects of the exact nature of the interaction between Si-nc and Er are still controversial. In principle, even

with the absence of an enhanced emission cross section, and provided that all Er could be inverted, the potential benefits of the Si-nc and Er codoping would still remain, thanks to the huge absorption cross section of Si-nc. However, for a reported effective excitation cross sections of Er $\sigma_{\text{eff}} \sim 2 \times 10^{-16} \text{ cm}^2$ (i.e., that of Si-nc)²³ and PL lifetimes $\tau_{\text{Er}} \sim 5 \text{ ms}$ one would expect to get optical transparency (inversion of 50% of Er ions within a quasi-two-level system) for pumping with $\sim 1 \times 10^{18} \text{ photons cm}^{-2} \text{ s}^{-1}$ ($\varphi_{1/2} = 1 / \sigma_{\text{eff}} \tau_{\text{Er}}$). Thus, the proportion of inverted Er reported so far needs to be greatly improved, especially those benefiting from the sensitizing action of Si-nc. The main aim of this paper is to address in depth the physics of this problem and attempt an explanation of such a strong Er quenching when excited through the Si-nc. Several authors have suggested different channels for the quenching of the Er emission, such as cooperative up conversion (CUC),¹⁵ excited-state absorption (ESA)²⁴ and Auger deexcitation but, as we shall show afterwards, even though being important, none of these mechanisms accounts for the small fraction of excitable Er through the Si-nc. An alternative (or additional) explanation was recently reported by us in Ref. 25. A short-range distance-dependent interaction between the Si-nc and the Er, and a small amount of sensitizers (Si-nc) are shown as the main limiting factors. A short-range, Auger-type kind of interaction is typical between semiconductors and dopant impurities, while the interaction between rare earths in silica (e.g., up conversion or energy migration) is a long-range dipole-dipole one.

Hence, this paper is an attempt to address the complicated nature of the interaction between Si-nc and Er in SiO_2 from both an experimental and theoretical point of view. It is done with the aim of answering the important question of how many Er ions are coupled to the Si-nc and the impact of this issue on the maximum attainable gain. Section II reports on sample preparation, compositional and morphological studies, including quantification of the density of Si-nc. Section III introduces rate-equation modeling of the most relevant interactions. Section IV reports detailed optical results and quantification of the amount of Er that can be excited via Si-nc, limited to about 2%, in the most favorable case. Different quenching mechanisms are considered and, despite being of considerable importance, fail to explain such low value of excitable Er. Section V develops a model for the interaction, based on the fact that the Si-nc and Er interaction is essentially of short-range exponential nature, with a characteristic distance of about 0.4 nm. The physics and modeling of this interaction is discussed in detail. We demonstrate that the energy transfer coefficient between Si-nc and Er depends on the Si-nc/Er distance and, therefore, is strongly dependent on the excitation flux. Thus, only those Er in close proximity to the Si-nc can be excited and the amount of excitable Er heavily depends on the Si-nc density (few 10^{17} cm^{-3}). For such a low Si-nc density the model predicts an Er excitable fraction in the range of a few percent, as we experimentally quantified. Finally, conclusions in Sec. VI account for the low density of sensitizers (Si-nc) and the short range of the interaction as the prominent explanation of the low fraction of Er coupled.

TABLE I. Main physical parameters of the samples studied within this chapter. Si excess and Er content were determined from RBS measurements.

Annealing time	Time	Si excess (at.%)	N_{Er} ($\times 10^{20} \text{ cm}^{-3}$)	Thickness (nm)	Refractive index
900 °C	60'	7	4.0	750	1.545
900 °C	30'	7	5.4	840	1.516
900 °C	10'	7	6.5	855	1.482
900 °C	5'	7	6.5	890	1.468
900 °C	1'	7	5.3	880	1.463

II. EXPERIMENT

A. Sample fabrication

A series of Er-doped Si-rich silica layers were deposited by reactive magnetron cosputtering on thermal silicon oxide grown on Si substrates. The Er content ($\sim 4\text{--}6 \times 10^{20} \text{ cm}^{-3}$) was adjusted through the number of the cosputtered Er_2O_3 pellets placed on top of the silica target, while the Si excess (6–7 at. %) was adjusted by the H content ($r_{\text{H}}=60\%$) in the plasma (mixed with Ar). The total plasma pressure was kept at 10^{-2} Torr. The Si substrates were not intentionally heated during the deposition. The H content in the plasma was found critical for the efficiency of the Er emission as it increases the density of nucleation centers and the concentration of Si-nc.²⁶ Annealing at 900 °C was found to maximize Er PL emission, while keeping amorphous all the Si precipitates.²⁶

Thus, the layers studied in this work belong to a series of samples optimized to find a compromise between (i) maximizing Er PL emission and lifetime and (ii) reducing carrier absorption to minimize optical losses in waveguides. The samples were annealed at 900 °C under N_2 flux for different durations, from 1 min up to 60 min. The increase of annealing time provided Si-nc with increased size so that long thermal treatments promoted complete phase separation.²⁷ A comprehensive study of the signal enhancement on waveguides fabricated with these same materials is provided elsewhere.^{20,27} The samples under study and their characteristics are summarized in Table I. The Si, O, and Er content have been determined by Rutherford backscattering spectroscopy (RBS) measurements. Thickness and refractive index were measured by m -lines spectroscopy.

B. Quantification of the density of Si-nc

An accurate determination of the amount of clusters is extremely important, as any physical modeling of the coupled Si-nc and Er ions system requires quantification of both of them. It has been obtained from an in-depth study of the energy-filtered transmission-electron-microscopy (EFTEM) pictures. The average diameter of the Si clusters is estimated around 3.2 nm. Nevertheless, the density of clusters in the field of view of the objective is too low for a direct estimation of the density. Dedicated samples with higher Si excess (15–25 at. %) have been prepared and studied for quantification. A typical EFTEM picture is shown in Fig. 1.

We used an electron probe diameter of about 2.5 nm to obtain the electron energy loss spectra (EELS) from 0 to 100 eV at the marked points in the EFTEM micrograph in Fig. 1. No objective aperture was used and the collection semiangle β was of about ~ 100 mrad. The value of convergence semiangle α is irrelevant as it is smaller than β when working in image mode without objective aperture.

We used the GATAN digital micrograph (DM) software to calculate the layer thickness from the EELS spectra, obtaining 52, 36, 34, and 39 nm at point 1, 2, 3 and 4, respectively. The window delimited between these points has a dimension of 87×88 nm. The total analyzed volume can be calculated using these data and corresponds to $3.08 \times 10^{-16} \text{ cm}^3$. Then, we counted the number of precipitates found within this volume and deduced the density of precipitates per volume unit, d_v . In this case $d_v = 5 \times 10^{17} \text{ cm}^{-3}$ (the uncertainty in the value is below 35%). Taking this value into account we can estimate for the samples studied in this work an upper value of $3 \times 10^{17} \text{ cm}^{-3}$ for the Si-nc density. The values obtained here are similar to those obtained by Iacona *et al.*²⁸ in samples with similar Si excess. In a recently published paper, Izeddin *et al.*²⁹ have measured the density of sensitizers (Si-nc) by optically pumping with intense laser pulses of a few ns, a shorter duration than the transfer time of the excitation ($\sim 1 \mu\text{s}$). Hence, by quantifying the emitting Er they deduce

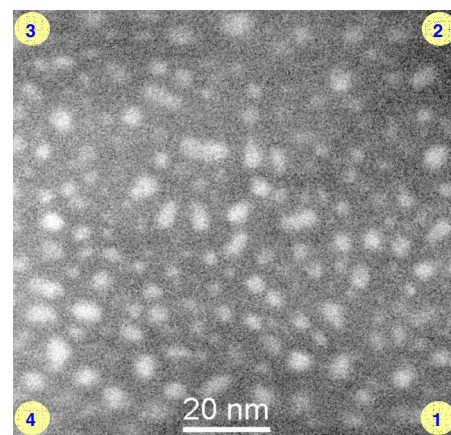


FIG. 1. (Color online) Energy filtered transmission electron microscopy (EFTEM) picture of one of the calibration samples used to determine the concentration of Si-nc. The numbers indicate the points where the thickness of the observed region has been determined from the electron energy loss (EELS).

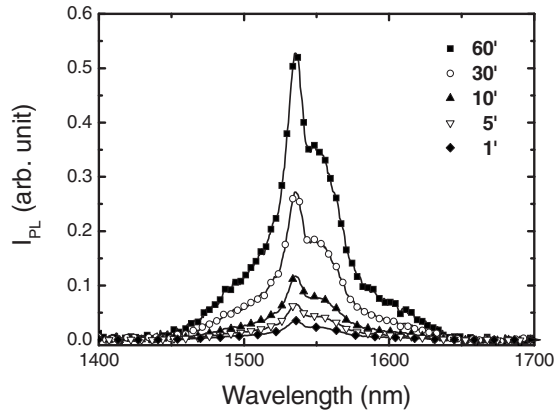


FIG. 2. Photoluminescence spectra obtained under 476 nm excitation for the five samples in the series, normalized to the layer thickness and erbium content.

about 3×10^{17} sensitizers/cm³, the same value we found by the EFTEM quantification. Such a coincidence is remarkable, even considering that the error bars are large (35%).

C. Photoluminescence spectra and lifetimes

PL emission was excited by the 488 nm and 476 nm lines of an argon laser modulated with a mechanical chopper to a frequency of 11 Hz. The spectra were taken with a thermoelectrically cooled InGaAs photomultiplier, connected to a lock-in to ensure synchronous detection. The 488 nm line is partially resonant with the transition between the ground state of the erbium and the level $F_{7/2}$ and has an absorption cross section of about 2×10^{-21} cm². The 476 nm line is, however, much less resonant and pumping at this wavelength ensures that almost all the Er ions are excited through the Si-nc. Figure 2 shows the spectra obtained with the 476 nm excitation, and normalized to the Er concentration and layer thickness, for the different annealing times. The samples with longer annealing duration show higher luminescence. This occurrence is attributed to the reduction of voids and defects and the increase in the fraction of Si excess precipitated into Si-nc.

Lifetime of the PL emission at $1.54 \mu\text{m}$ (τ_{PL}) was measured by connecting the InGaAs photomultiplier to a digital GHz oscilloscope. Figure 3 plots the τ_{PL} measured at a relatively low flux of about 10^{18} cm⁻² s⁻¹ for the different samples as a function of the annealing time. The values of Er³⁺ PL lifetimes at $1.54 \mu\text{m}$ as a function of the annealing time are also summarized in Table II. The emission lifetime increases with the annealing time, reaching almost 5 ms for the 60' sample. This improvement can be also related to the recovery of the matrix after the annealing of nonradiative defects. The importance of optimizing the annealing duration is apparent, as PL intensity and lifetime increase almost one order of magnitude between 1' and 60' treatments. High PL emission efficiency and long lifetime are fundamental requirements to obtain significant population inversion with minimum pump power and thus maximize optical gain.

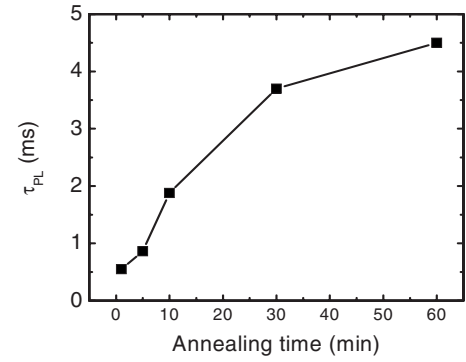


FIG. 3. Photoluminescence lifetime versus annealing time.

III. Er³⁺ LUMINESCENCE MODEL BASED ON THE INTERACTION BETWEEN Si-nc AND Er³⁺ IONS

Modeling using coupled rate equations is commonly reported in the literature to account for the excitation of Er in systems with sensitizers.^{3,15} The model used in this work is fundamentally based on the one of five levels of Er³⁺ ions interacting with a quasi-two-level scheme of Si-nc. A comprehensive description of the rate equations of such a coupled model for Si-nc and Er can be found in Ref. 15. Hereafter we will give a brief description of the model, together with the modifications adopted for the sake of simplicity. A simulator has been implemented to numerically solve the rate equations with the five levels of Er. While the physical insight is lost in the numerical simulations, the simplified versions provide a useful understanding on the basic interaction process.

Figure 4 schematically illustrates the interaction between Si-nc and Er³⁺ ions, and indicates the paths for excitations and deexcitations. As soon as a Si-nc, with its absorption cross section σ_{Si} , absorbs incident pump photons with a flux φ , carriers are generated, and eventually trapped at interfacial states that are below the conduction band of Si-nc. Due to the very fast capturing rate of carriers, the energy scheme of Si-nc can be regarded as a quasi-two-level system, and the exciton generating rate can be defined as $\sigma_{\text{Si}}\varphi$. If such excitons are isolated from Er³⁺ ions, they will recombine radiatively emitting visible light, or nonradiatively due to quenching centers nearby Si-nc, independently of Er³⁺ ions. Total decay time for such intrinsic Si-nc is defined as τ_{Si} [refer to the arrow marked as (a) in the figure]. When Si-nc are coupled to Er³⁺ ions, the recombination energy of excitons can be transferred to the Er³⁺ ions in the ground state promoting them to higher excited states [the arrow with (b)]. An additional mechanism that depletes the excited Si-nc has been considered: excited-state absorption (ESA), a process in which an excited Er is pumped to a higher excited level by the energy transfer from the recombination of an excited Si-nc [the arrow with (c)]. As a result, the rate equation for the Si-nc subsystem in the coupled system is

$$\frac{dN_{\text{Si}}^*}{dt} = \sigma_{\text{Si}}\varphi N_{\text{Si}}^0 - \frac{N_{\text{Si}}^*}{\tau_{\text{Si}}} - K_1 N_1 N_{\text{Si}}^* - K_2 N_2 N_{\text{Si}}^*, \quad (1)$$

where N_{Si}^* is the density of excited Si-nc, N_{Si}^0 is the Si-nc density in the fundamental state, and $N_{\text{Si}} = N_{\text{Si}}^* + N_{\text{Si}}^0$ is the

TABLE II. Experimental values of the total number of doped Er ions, the maximum excitable Er fraction, 1.54 μm Er^{3+} PL lifetimes, and the effective excitation cross section for the samples studied in this work.

Annealing time	N_{Er} ($\times 10^{20} \text{ cm}^{-3}$)	$N_{2 \text{ max}}$ ($\times 10^{18} \text{ cm}^{-3}$)	$N_{2 \text{ max}}/N_{\text{Er}}$ (%)	τ_{PL} (msec) ^a	σ_{eff} ($\times 10^{-17} \text{ cm}^2$) ^b
60'	4.0	7.02	1.76	4.5	0.73
30'	5.4	6.17	1.14	3.7	0.78
10'	6.5	2.35	0.36	1.9	1.40
5'	6.5	1.85	0.28	0.9	2.44
1'	5.3	0.70	0.15	0.6	3.12

^aAt φ of $\sim 10^{18} \text{ cm}^2/\text{s}$.

^bAt φ of $5 \times 10^{18} \text{ cm}^2/\text{s}$.

total number of Si-nc; K_1 is the coupling constant between Si-nc and Er in the ground state, and K_2 is the coefficient for ESA. It is worth noting that the recombination within the Si-nc and the energy transfer to Er ions (the second, third, and last term on the right-hand side) are competing mechanisms; N_2 and N_1 are the densities of the first excited and fundamental states of Er, respectively. We assume that strong and fast Auger interaction between excitons in a single Si-nc prevents the creation of more than one exciton per Si-nc in steady-state regime.

Let consider the dynamics of Er ions. The N_1 ions in the ground state are excited by energy transfer from excitons and the excited Er^{3+} at higher lying levels decay fast to the first excited state (within 1–2 μs). Similarly to Si-nc, these excited Er^{3+} ions can radiatively decay by emitting photons at 1.54 μm or nonradiatively decay due to quenching centers, if other deexcitation processes are negligible. Again such intrinsic Er^{3+} decay lifetime is described as τ_2 [see the arrows marked (i)]. One of the most frequently reported deexcitation processes is the cooperative up conversion (CUC) that concerns the interaction of two Er ions, both in the first excited level (${}^4I_{13/2}$). Such an interaction might result in the promotion of one ion to the third excited level (${}^4I_{9/2}$) and the deexcitation of the other to the ground state [the arrow marked (ii)]. Subsequently, the excited ion decays rapidly to the second level and then nonradiatively through the emission of phonons to the first excited level in few μs , or radiatively to the fundamental state with a low branching ratio (weak luminescence from the second excited level can be detected at

980 nm). Additionally, the deexcitation of N_2 by Auger excitation of excitons (AEE) is also included in our model. This deexcitation involves N_2 and N_{Si}^* similarly to ESA, but with the difference that the energy of N_2 is transferred to N_{Si}^* promoting them to a higher energy level [the arrow marked (iii)].

In fact, ESA and CUC populate other higher excited states of Er^{3+} ions (i.e., ${}^2H_{11/2}$ and ${}^4I_{9/2}$ for ESA and CUC, respectively). Additionally, it is still unclear to which state Er will be excited through the energy transfer from Si-nc, considering the controversy about the quasisonant excitation of Er^{3+} .³⁰ Because of that, the inclusion of higher excited Er^{3+} energy states, as in the base model suggested by Pacifici *et al.*, would make our model more accurate. Nevertheless, since the nonradiative transition rate of ${}^4H_{11/2} \rightarrow {}^4I_{9/2}$, ${}^4I_{9/2} \rightarrow {}^4I_{11/2}$, and ${}^4I_{11/2} \rightarrow {}^4I_{13/2}$ of Er^{3+} 4f energy levels are as fast as $\sim 1 \times 10^7$, $\sim 1 \times 10^7$, and $\sim 4 \times 10^5 \text{ s}^{-1}$, respectively, the Er^{3+} ions in other higher excited states are expected to be quickly relaxed to the first excited state. This implies that Er^{3+} ions exist mainly either in the ground state or in the first excited state during the interaction with Si-nc, allowing us to regard the energy scheme of Er^{3+} as a quasi-two-level system for practical purposes. In this way, we can assume that the CUC effect will cause the depletion of only one Er^{3+} ion, of the two involved in the process.

As a result, the rate equation for Er^{3+} ions in the first excited state in the coupled system for a quasi-two-level scheme is

$$\frac{dN_2}{dt} = K_1 N_{\text{Si}}^* N_1 - \frac{N_2}{\tau_2} - C_{\text{up}} N_2^2 - C_A N_{\text{Si}}^* N_2, \quad (2)$$

where C_{up} and C_A are the CUC and AEE coefficients, respectively. The total number of Er ions N_{Er} now becomes equal to N_1 plus N_2 ($N_{\text{Er}} = N_1 + N_2$). The last three terms of the right-hand side of Eq. (2) indicate that the intrinsic decay, CUC, and AEE induced deexcitation will compete with each other in the deexcitation process of the excited Er^{3+} ions.

Moreover, by comparing the dynamics of excited Si-nc and excited Er^{3+} ions, one will deduce that the overall process of photogeneration of excitons in Si-nc plus energy transfer to Er^{3+} ions is much faster than the excitation and deexcitation of Er^{3+} ions. Because of that, when the pump flux is raised, Si-nc will very quickly reach the steady-state equilibrium and its rate equation becomes equal to zero.

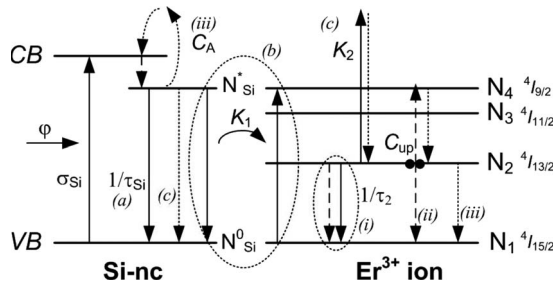


FIG. 4. Schematic description for the interaction model between Si-nc and Er^{3+} ions, and the excitations and deexcitations of them. The model of energy level both for Si-nc and Er^{3+} ions was regarded as a quasi-two-level system in the modeling equations.

Thus, it is more convenient to handle the dynamics of Er^{3+} by introducing their own effective excitation cross section σ_{eff} instead of dealing with Si-nc and Er^{3+} , individually. This assumption allows one to write

$$\frac{dN_{\text{Si}}^*}{dt} \rightarrow 0,$$

$$\frac{dN_2}{dt} = \sigma_{\text{eff}}\varphi N_1 - \frac{N_2}{\tau_2} - C_{\text{up}}N_2^2 - C_A N_{\text{Si}}^* N_2, \quad (3)$$

where

$$\sigma_{\text{eff}} \approx \sigma_{\text{Si}} \frac{K_1 N_{\text{Si}}}{\sigma_{\text{Si}}\varphi + \frac{1}{\tau_{\text{Si}}} + K_1 N_1 + K_2 N_2}. \quad (4)$$

Note that all parameters of Eq. (4) are derived from Eq. (3) (the steady state of Si-nc), and N_1 and N_2 in steady state are consequently time independent, but a function of the pump flux. A detailed discussion about σ_{eff} will be provided in the following section.

By analyzing the low pump flux regime, it is clear that most Er^{3+} ions are at the ground state and related deexcitation processes of excited Er^{3+} are small. Then excited Er^{3+} ions are expected to monotonically decay with the experimentally measured PL lifetime τ_{PL} that includes as second order terms the CUC and AEE (we used τ_{PL} in order to distinguish it from the intrinsic decay τ_2). In such a case, Eq. (3) is simplified to

$$\frac{dN_2}{dt} = \sigma_{\text{eff}}\varphi N_1 - \frac{N_2}{\tau_{\text{PL}}}. \quad (5)$$

In steady-state conditions ($dN_2/dt=0$), the population of excited Er^{3+} in the low pump regime is finally given by

$$N_2 = \frac{N_{\text{Er}}\varphi}{\varphi + \frac{1}{\sigma_{\text{eff}}\tau_{\text{PL}}}}, \quad (6)$$

which is the typical sigmoidal curve that defines the population of a simplified two-level system. Note that even at high pump flux σ_{eff} has the physical meaning of a cross section for Er excitation and τ_{PL} of Er deexcitation time, although they will be flux dependent when other deexcitation processes start to affect N_2 .

IV. RESULTS AND DISCUSSION

A. Density of excited Er and effective excitation cross section

Quantitative measurements of the photon flux emitted by the samples were performed by using a reference calibrated sample whose emission has been independently evaluated and quantified. This sample was a soda-lime glass, 1.3 mm thick, supplied by Corning Inc., doped with Er^{3+} to a density of $2 \times 10^{20} \text{ cm}^{-3}$. The large thickness ensures that PL emission, upon 488 nm excitation, can be directly measured with a calibrated optical multimeter, coupled to an integrating sphere. Geometrical, absorption, and internal reflection ef-

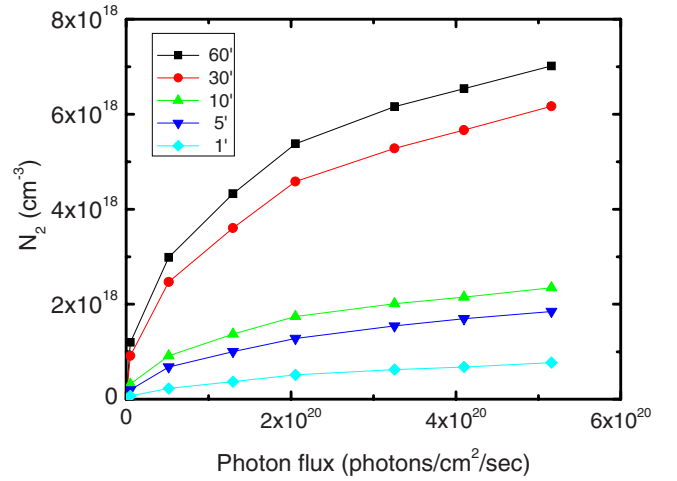


FIG. 5. (Color online) Population of the level $^4I_{13/2}$ of Er under 476 nm excitation for the series of samples used in this work.

fects were carefully considered, in order to determine the actual emission of the sample. At a pump flux $\varphi = 1.3 \times 10^{20} \text{ cm}^{-2} \text{ s}^{-1}$, the emission of the reference sample was found to be 0.598 mW, corresponding to a density of excited Er^{3+} ions equal to $6.3 \times 10^{17} \text{ cm}^{-3}$. This value is quite close to the expected one, as calculated from the rate equation (for direct excitation of Er the used photon flux can be considered as low) as follows:

$$N_2 = \frac{N_{\text{Er}}\varphi}{\varphi + \frac{1}{\sigma_{488}\tau_{\text{PL}}}} \approx N_{\text{Er}}\sigma_{488}\tau_{\text{PL}}\varphi = 4.2 \times 10^{17} \text{ cm}^{-3}. \quad (7)$$

For the calculation we have used the measured lifetime $\tau_{\text{PL}} = 8 \text{ ms}$ and $\sigma_{488} = 2 \times 10^{-21} \text{ cm}^2$. The agreement demonstrates that the calibration is correct. Using the calibrated sample as a reference, we were able to determine the collection losses and detector response in our PL setup, allowing the conversion of the photomultiplier signal into the emitted photon flux, which, in turn, is related to N_2 through

$$\sigma_{\text{emitted}} = \frac{N_2}{\tau_{\text{rad}}} Ad, \quad (8)$$

where d is the layer thickness, A is the illuminated area, and τ_{rad} is the radiative lifetime, a parameter determined by Dal-dosso *et al.* on the same set of samples.²⁰ For the sample annealed at 60', τ_{rad} takes the highest value of 10 ms. This value is smaller than the one in SiO_2 (18 ms), which has a lower refractive index than silicon-rich silica. The samples were excited with the 476 and 488 nm lines of an Ar laser, to a maximum laser power of 215 and 430 mW, respectively. Since the dimension of the laser spot depends on the emitted power, we maintained the spot size on the samples at $\sim 10^{-3} \text{ cm}^2$ by keeping maximum and constant the laser emission and modifying its intensity on the sample by a set of neutral density filters.

Hence, from PL measurements we were able to calculate the absolute value of N_2 for each sample, as plotted in Fig. 5 against photon flux for the nonresonant 476 nm excitation.

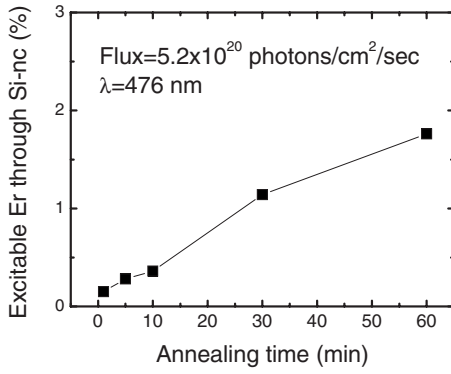


FIG. 6. Maximum percentage of Er indirectly excitable through the Si-nc for the highest pumping power used in this work as a function of annealing time.

These values are slightly lower than those reported by us in Ref. 25, as at that preliminary stage we used τ_{rad} of SiO_2 , while here we take the τ_{rad} of each sample. The maximum density of excited Er obtained is $7 \times 10^{18} \text{ cm}^{-3}$ (1.76%), at the highest flux of $5.2 \times 10^{20} \text{ cm}^{-2} \text{ s}^{-1}$, for the longest annealed sample (60'). This is for the best performing sample, whereas for the others the fraction of excited Er at the maximum flux was much lower, as shown in Fig. 6 and reported in Table II. All these low values of the indirectly excitable Er at maximum power indicate that a strong limiting phenomenon is taking place. By using the excitation cross section of Si-nc ($\sim 10^{-16} \text{ cm}^2$) and the lifetime of the best performing sample ($\sim 5 \text{ ms}$), one would expect for a two-level system that transparency, i.e., 50% of excited Er, would occur at $1/\sigma\tau \sim 10^{18} \text{ cm}^{-2} \text{ s}^{-1}$, as to say two orders of magnitude less than the maximum flux used in this experiment for which one gets only 1.76% of Er excited.

In Eq. (6) N_{Er} should be now replaced by $N_{2 \text{ max}}$ that represents the maximum Er^{3+} population excitable through Si-nc, since the presented results clearly show that not all the Er^{3+} ions in the films are accessible by Si-nc. Even though the exact value of $N_{2 \text{ max}}$ is unknown, as it will be discussed in Sec. V, from Figs. 5 and 6 we assumed that the experimental values of the density of excited ions at the highest pump flux ($5.2 \times 10^{20} \text{ cm}^{-2} \text{ s}^{-1}$) are close to $N_{2 \text{ max}}$ in order to roughly predict some parameters in the Er^{3+} excitation dynamics. By combining Eq. (6) together with the experimental values of $N_{2 \text{ max}}$ and τ_{PL} the effective excitation cross section gets $\sigma_{\text{eff}} = 7.34 \times 10^{-18} \text{ cm}^2$ for the 60' annealed sample pumped at $\varphi = 5 \times 10^{18} \text{ cm}^{-2} \text{ s}^{-1}$. This estimation is more than one order of magnitude lower than the expected excitation cross section of Si-nc, confirming that at that relatively small flux quenching or limiting phenomena are already taking place. For the rest of the samples, the effective excitation cross section increases to a certain amount. The highest value is for sample annealed 1', $\sigma_{\text{eff}} = 3.1 \times 10^{-17} \text{ cm}^2$ at the same flux, so all the measured values range within a factor of 4. The amount of Si excess is the same for all samples, and it appears that the additional annealing duration reduces the coupling strength (i.e., σ_{eff}). We speculate that for samples with a larger excitable Er fraction, σ_{eff} is an average over a larger amount of Er ions and not

only on those in favorable position for the energy transfer (afterwards we will come back to this point in more detail). The results also show that annealing duration significantly increases the amount of Er ions coupled to the Si-nc, probably by eliminating voids and defects that otherwise quench the energy transfer and this is precisely the reason why the Er lifetime increases with annealing time. In Table II we have summarized the maximum amount of excitable Er, its percentage with regards to the total Er content, and the effective excitation cross section at nonresonant excitation (476 nm) and at a flux $\varphi = 5 \times 10^{18} \text{ cm}^{-2} \text{ s}^{-1}$.

We have also performed time-resolved luminescence experiments on samples annealed at 60' 30', and 10' to obtain the effective excitation cross section at lower fluxes, in the range of $10^{16} - 10^{18} \text{ cm}^{-2} \text{ s}^{-1}$. By using the common expressions for a two-level system, the rise (τ_r) and decay (τ_{PL}) times are related by

$$\frac{1}{\tau_r} - \frac{1}{\tau_{\text{PL}}} = \sigma_{\text{eff}} \varphi. \quad (9)$$

The results, as expected from the data above, show that σ_{eff} is similar for all the samples studied here, but the values clearly depend on the photon flux used for excitation. For very low photon fluxes ($\sim 10^{16} \text{ cm}^{-2} \text{ s}^{-1}$), all the effective excitation cross sections are close to the values expected for Si-nc, i.e., $\sigma_{\text{eff}} = 0.7 - 1 \times 10^{-16} \text{ cm}^2$. However, for fluxes of the order of $10^{17} \text{ cm}^{-2} \text{ s}^{-1}$, $\sigma_{\text{eff}} \approx 2 \times 10^{-17} \text{ cm}^2$ (60, 30, and 10' samples). Comparing with the results reported above for $5 \times 10^{18} \text{ cm}^{-2} \text{ s}^{-1}$, one observes that the effective excitation cross section roughly decreases one order of magnitude per decade of increasing flux. Thus, Si-nc to Er energy transfer quenches with increasing flux.

B. Si-nc and Er^{3+} interactions

1. Effect of excited state absorption (ESA)

As expressed in Eq. (4), σ_{eff} is a function of φ indicating that excitation efficiency will be affected by large values of φ . In fact, at low pump fluxes since most Er^{3+} ions are in the ground state ($N_2 \ll N_1$), σ_{eff} is assumed to be almost constant as $\sigma_{\text{eff}} \approx \sigma_{\text{Si}} K_1 N_{\text{Si}} / (1/\tau_{\text{Si}} + K_1 N_1)$. On the other hand, as φ increases, the exact correlation between σ_{eff} and φ appears unclear, since both N_1 and N_2 are the values at steady state and thus are also φ dependent, while the first two terms in the denominator of Eq. (4) are straightforward. In spite of the uncertainty about the correlation between σ_{eff} and φ , the increase of φ populates N_2 and strengthens ESA effect, resulting in a decrease of σ_{eff} . Thus even though ESA does not involve the depopulation of N_2 (since Er^{3+} ions affected by ESA are quickly relaxed back to the first excited state), it can definitely act as a limiting effect on Er at high φ , from the correlation between N_2 and σ_{eff} as shown in Eq. (4). The other parameter that plays an important role in σ_{eff} is K_1 . If the interaction is dependent on the Si-nc to Er distance, ions excited at higher flux are on less favorable position and will have a lower K_1 (and K_2) and this will cause a drop in σ_{eff} as well. For the moment we keep K_1 and K_2 independent on distance (flux) and analyze if ESA, CUC, and AEE alone can

explain the low amount of excited Er. Although ESA involves an isolated Er and is not dependent on the Er concentration, actually it strongly depends on φ and the absorption cross section of the excited level to the pumping photons. Some recent reports have emphasized the importance of ESA, pointing out the resonant character of the energy transfer from Si-nc to Er at around 750 nm (emission of Si nanocrystals), for which the excited level N_2 has a significant cross section.²⁴

As shown in Eq. (4) again, σ_{eff} is determined by the competition between the energy transfer to Er^{3+} and the ESA effect. Thus the comparison between these two phenomena (K_2N_2/K_1N_1) will reveal the predominance of the ESA effect in Er^{3+} excitation or deexcitation dynamics. In order to consider an extreme case, one can consider the sample annealed 60' for which the maximum concentration is $N_2=7 \times 10^{18} \text{ cm}^{-3}$ and $K_2=1 \times 10^{-15} \text{ cm}^3/\text{s}$, as to say the largest value ever reported (Ref. 24). This latter value is used even though it is similar to $K_1=3 \times 10^{-15} \text{ cm}^3/\text{s}$ (Ref. 15) and much larger than K_2 of less than $3 \times 10^{-19} \text{ cm}^3/\text{s}$ (see also Ref. 15).

Finally, the ratio K_2N_2/K_1N_1 is found to be as low as 5.9×10^{-3} . Hence, the impact of ESA in the effective excitation cross section for such a low population of excited Er is negligible if we consider all the Er population coupled to the Si-nc. Nevertheless, as K_1 and K_2 get comparable in these calculations, ESA can have a significant impact once a high population inversion is achieved and its main effect will be a shift in the transparency limit to higher pumping powers. As for transparency $N_1=N_2$, if one makes comparable both coefficients $K_1 \approx K_2$, then ESA will at most shift the transparency limit by a factor of 2 in the required pumping flux.

2. Effect of cooperative conversion

Cooperative up conversion (CUC) has been previously studied in SiO_2 doped with Si-nc and Er by a certain number of authors^{15,17} and is known to play a significant role when both or either Er concentration and/or pumping flux are high. As stated above, CUC refers to the interaction of two Er ions in the first excited level, resulting in one remaining in the first excited state (after a few μs of decay from upper levels) and the deexcitation of the other to the fundamental level. The first excited state will be, therefore, depleted and thus CUC can affect significantly the pumping flux regime needed for population inversion. CUC is usually modeled through the up-conversion coefficient C_{up} as indicated above.

$$\frac{dN_2}{dt} = \sigma_{\text{eff}}N_1\varphi - \frac{N_2}{\tau_2} - C_{\text{up}}N_2^2. \quad (10)$$

The approximate quasi-two-level model is justified by the fact that the N_4 level populated by CUC returns to the first excited state in 1 μs at most, i.e., three orders of magnitude lower than the ms lifetime for N_2 .

When pump beam is turned off ($\varphi=0$), Eq. (10) is now simplified as

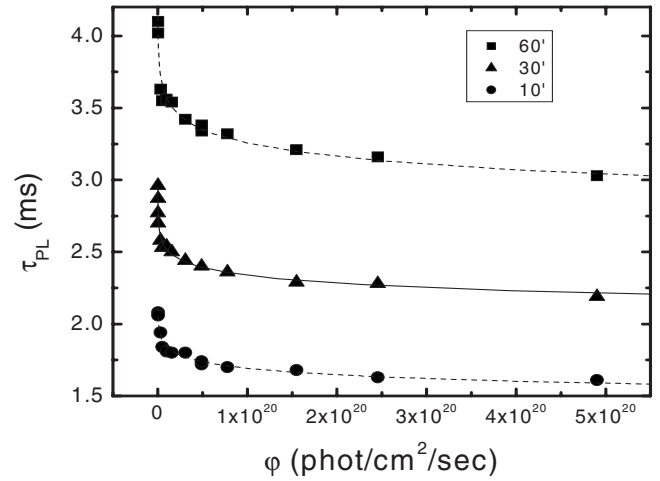


FIG. 7. Dependence of the lifetime with the pumping flux for samples annealed at 60', 30', and 10'.

$$\frac{dN_2(t)}{dt} = -\frac{N_2(t)}{\tau_2} - C_{\text{up}}N_2^2(t). \quad (11)$$

Note that N_2 is a function of time and the CUC process involves two excited erbium ions at the same time. After analytical calculation, a time-dependent normalized number of excited Er^{3+} ions $f(t)$ is found as follows:

$$\frac{N_2(t)}{N_2(0)} = \frac{\exp\left(-\frac{t}{\tau_2}\right)}{1 + C_{\text{up}}\tau_2N_2(0)\left[1 - \exp\left(-\frac{t}{\tau_2}\right)\right]} = f(t). \quad (12)$$

We now define the PL lifetime τ_{PL} as the integrated value of $f(t)$ from $t=0$ to ∞ (a single exponential with the same area).

$$\tau_{\text{PL}}(\varphi) = \int_0^\infty \frac{N_2(t)}{N_2(0)} dt = \frac{\ln[1 + N_2(0)\tau_2C_{\text{up}}]}{N_2(0)C_{\text{up}}}. \quad (13)$$

Note that τ_{PL} is a function of φ since $N_2(0)$ is also φ dependent.

Figure 7 shows the dependence of the lifetime with the pumping flux at nonresonant excitation (476 nm) for the three most emitting samples (60', 30', and 10' annealing time). A strong decrease of the lifetime is observed in all three samples, followed by some stabilization for pump powers over $10^{20} \text{ cm}^{-2} \text{ s}^{-1}$. For comparison (not shown) we also pumped the soda-lime bulk reference sample and we could not detect variations in the Er lifetime for that range of fluxes. Figure 8 compares the evolution of the PL decay rate with the density of inverted ions, to that expected from Eq. (13). The only fitting parameter is the C_{up} coefficient and the agreement between experimental and calculated data implies that CUC is indeed responsible for the observed variation in the lifetime versus the pump power. A simplified version of Eq. (13) is deduced from the rate equation of Eq. (10) as $1/\tau_{\text{PL}} \sim 1/\tau_2 + C_{\text{up}}N_2$, which emphasizes the linear dependence shown in Fig. 8. The up-conversion coefficients in our set of samples have been estimated by a linear regression of

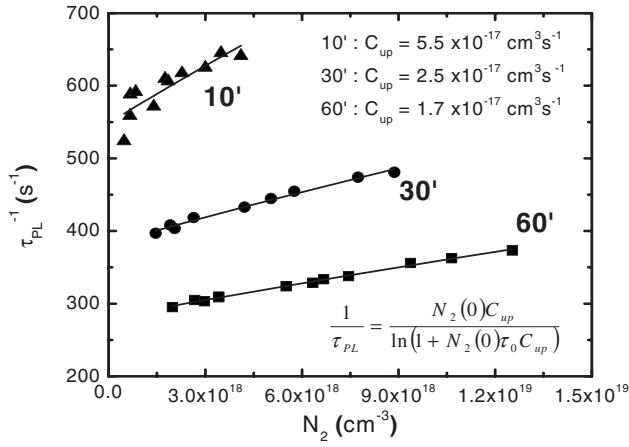


FIG. 8. Inverse of the PL lifetime plotted against the density of excited Er ions and the up-conversion coefficients.

the curves in Fig. 8. The values obtained are between 1.7 and $5.5 \times 10^{-17} \text{ cm}^3 \text{ s}^{-1}$, with the lowest value corresponding to the longest annealing duration ($60'$). These C_{up} values are consistent with previous results from Er-doped Si-nc embedded in SiO_2 .¹⁵

Let us evaluate now the role of CUC in quenching the Er excitation for the $60'$ sample as an example. After Eq. (10), the contribution of CUC to the rate equation is $C_{\text{up}}N_2^2$ and competes with the intrinsic deexcitation N_2/τ_2 . For the highest flux (when excited Er reaches its maximum) the deexcitation to the fundamental state is still higher than the up-conversion term by roughly a factor of 2. Consequently, CUC is playing a significant role in depleting N_2 but it cannot account for the extremely low fraction of excitable Er (1.76%).

An interesting way to examine the CUC mechanism is to evaluate how it affects the pumping flux needed for transparency (50% inversion of Er). By exactly solving Eq. (10) for steady state it is found that C_{up} stretches the typical sigmoidal curve of Eq. (6). The net effect of CUC is to significantly increase the pumping flux needed for transparency and gain. By neglecting C_{up} the flux for transparency would be just $\varphi_{1/2} = 1/\sigma_{\text{eff}}\tau_2$, while with C_{up} it turns out to be

$$\varphi_{1/2} = \frac{1}{\sigma_{\text{eff}}\tau_2} \left(\frac{1}{2} N_{\text{Er}} C_{\text{up}} \tau_2 + 1 \right). \quad (14)$$

By inserting in Eq. (14) the parameters of the $60'$ sample, one finds that the transparency flux is $\varphi_{1/2} \approx 2.5 \times 10^{18} \text{ cm}^{-2} \text{ s}^{-1}$ without considering without up conversion, while it becomes $\varphi_{1/2} \approx 3.5 \times 10^{19} \text{ cm}^{-2} \text{ s}^{-1}$, roughly one order of magnitude higher, when it is included. Thus, for a material with 100% of excitable Er, up conversion will be a matter of serious concern. Including the effect of ESA calculated in the previous section, the transparency limit with CUC and ESA combined will be shifted to almost $1 \times 10^{20} \text{ cm}^{-2} \text{ s}^{-1}$. Finally, we have tried to reproduce N_2 as a function of pumping flux (results plotted in Fig. 5), by solving Eq. (10) in steady-state regime and using the values calculated for σ_{eff} , C_{up} , and τ_2 . The results are displayed in Fig.

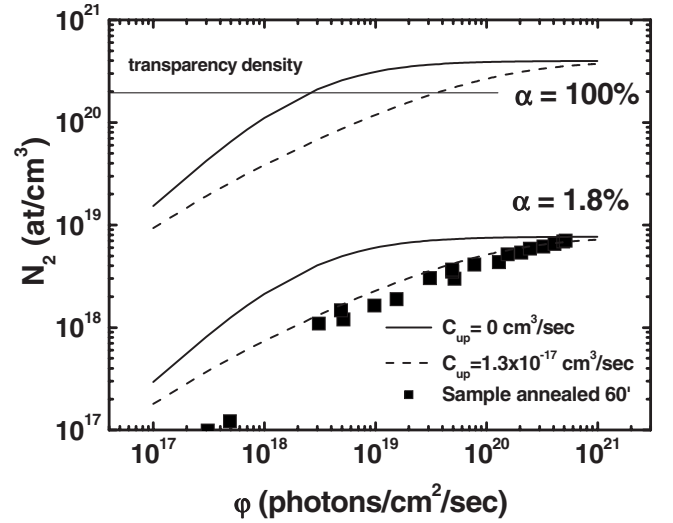


FIG. 9. Experimental data and simulation of the number of Er atoms in the excited state for a sample annealed at $60'$. Solid curves account for the evolution without up conversion and a different percentage of Er coupled to the Si nanoclusters. Dashed curves included up-conversion effects.

9. The experimental $N_2(\varphi)$ can be reproduced quite well only if one introduces an *ad hoc* factor that reduces the amount of Er indirectly excitable by the Si-nc to roughly 1.8%. The graph also displays the curves with and without CUC if 100% of the Er were excitable through the Si-nc. The shift of the flux needed for transparency is shown for the curve with up conversion.

3. Effect of Auger deexcitations

In principle, the evolution of lifetimes in Figs. 7 and 8 could be also explained by an Auger effect (AEE), a non-radiative deexcitation of excited Er ions giving back the energy to excitons in the Si-nc. However, when the pump beam is turned off, the excitons recombine within a few μs while excited Er ions decay within a few ms, making difficult any estimate of AEE effect from Er^{3+} PL decay traces. However, in steady-state conditions, excitons always exist and an Auger effect is expected to be rather active, especially for high pump regime where the population of excitons becomes very dense. Although detailed investigations are needed, such as the double-pulse pumping, to deeply investigate the Auger effect,³⁰⁻³² we introduce here a simple approach to examine the weight of AEE among other deexcitation processes of excited Er^{3+} ions.

The last three terms in Eq. (3) can be rewritten as

$$-N_2 \left(\frac{1}{\tau_2} + C_{\text{up}}N_2 + C_A N_{\text{Si}}^* \right). \quad (15)$$

Note that the terms between parentheses in Eq. (15) reflect different deexcitation processes: excited Er^{3+} ions including CUC with $C_{\text{up}}N_2$ and Auger deexcitation with $C_A N_{\text{Si}}^*$. Apart from $1/\tau_2$, which is assumed to be invariant on either φ and N_{Er} , the predominance of the Auger effect over CUC ($C_A N_{\text{Si}}^* > C_{\text{up}}N_2$) requires a population of excited Si-nc more

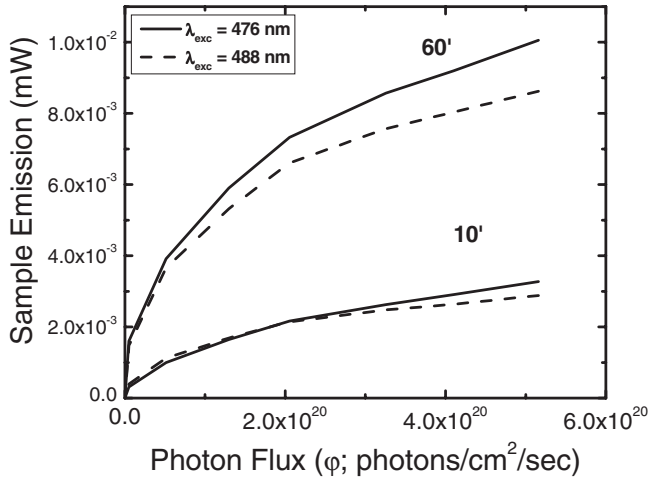


FIG. 10. Emission of the samples annealed at 60' and 10', as a function of the pump photon flux, for resonant (488 nm) and non-resonant (476 nm) excitation.

than two orders of magnitude higher than that of excited Er^{3+} ions, assuming a comparable magnitude of C_A and C_{up} . For example (see Fig. 5), almost 10^{18} Er cm^{-3} can be usually excited in a moderate pump regime ($\sim 10^{19}$ $\text{cm}^{-2} \text{s}^{-1}$), implying the CUC rate as high as ~ 10 s^{-1} .

On the other hand, when the value of C_A for Er-doped Si-nc is assumed to be $\sim 10^{-19}$ $\text{cm}^3 \text{s}^{-1}$ (Ref. 15), the maximum deexcitation rate by the Auger effect rarely exceeds 10^{-2} s^{-1} even when all Si-nc are excited. This value is much smaller than $1/\tau_2$, which is >200 s^{-1} for our films, and even smaller than the CUC rate as well. Furthermore, K. Imakita *et al.*³³ reported a measurement of the Auger coefficient directly from the PL decays after doping the Si-nc with shallow impurities (*P* or *B*). They got an upper value of $C_A = 6.1 \times 10^{-17}$ $\text{cm}^3 \text{s}^{-1}$. Even by assuming that the interaction of an excited Er with an exciton is comparable to that of the shallow impurity, the resulting Auger deexcitation rate is about 2 s^{-1} , still much lower than the CUC. Thus we believe that the Auger effect is not as active as the CUC in the steady-state regime, and does not considerably represent a limiting factor for the determination of excited Er^{3+} ions numbers.

C. Optically active Er ions

1. Direct absorption versus indirect excitation

The PL experiment was repeated under the exact same conditions with the resonant 488 nm line. The resulting total emission versus flux is slightly higher than that for the 476 nm line. The comparison between the two excitations is shown for samples annealed for 60' and 10' in Fig. 10. While the PL emission tends to saturate under high nonresonant pumping, it continues growing rather linearly when pumped with the 488 nm line. This is observed in all samples, and allows one to infer that, while the energy transfer from the Si-nc tend to quench at high flux, Er can still be directly excited by the 488 nm line. This finding is of great importance, as it indicates that the quenching problem is not

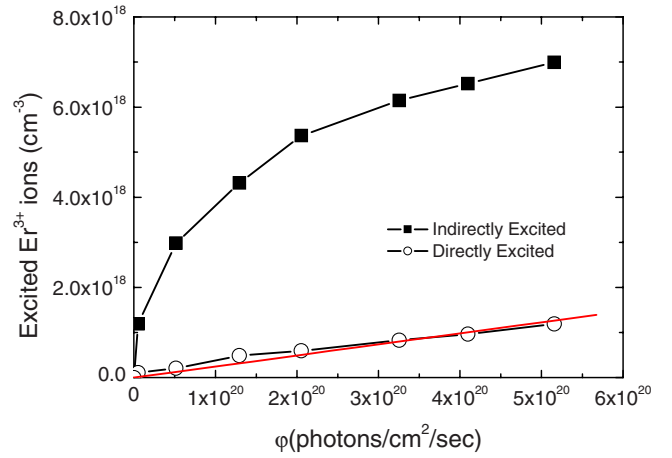


FIG. 11. (Color online) Contribution of the direct and indirect excitation to the density of excited Er ions when pumping at 488 nm after subtracting the excitation at 476 nm.

residing in an eventual inactive character of the Er population, but rather in the ineffectiveness of the energy transfer.

The comparison between resonant and nonresonant excitation allows one to calculate the fraction of optically active ions in the sample, which we define as the amount of Er that can be excited resonantly. For doing this, we have just subtracted the population N_2 of the first excited level after excitation with 488 nm from that after 476 nm pumping ($N_{2@488} - N_{2@476}$). Assuming that the amount of Er excited via the Si-nc is the same when pumping at 488 and 476 nm, this subtraction will separate the contributions of directly and indirectly excited Er. This subtraction is shown in Fig. 11 for the sample annealed 60' and results in a straight line, $N_2 = N_{\text{Er}} \sigma_{488} \tau_{\text{PL}} \phi$, as expected for direct excitation at low pumping (transparency for direct pumping is accomplished at a flux of about $1/\sigma_{488} \tau_{\text{PL}} \sim 10^{23}$ $\text{photons/cm}^2 \text{s}$, i.e. much higher than the one used here).

Due to the broad $\text{Er}^{3+} {}^4F_{7/2} \rightarrow {}^4I_{15/2}$ absorption band peaking at ~ 488 nm, it is also possible that some Er ions can be resonantly excited even under 476 nm pumping. However, we found a much smaller σ_{476} optical absorption cross section of Er ions at 476 nm, as low as $\sigma_{476} \sim 10^{-22}$ cm^2 , as evaluated from PL and visible absorption measurements on Er-doped glasses. This allowed one to neglect the contribution of excited Er ions by direct optical absorption under a 476 nm pump. In fact, by including the contribution under a 476 nm pump, but almost the same results were drawn. The linear fitting of this subtraction allows one to obtain N_{Er} , here the total amount of optically active Er. The slope of the fit ($N_{\text{Er}} \sigma_{488} \tau_{\text{PL}}$) is $\sim 2.4 \times 10^{-3}$ s cm^{-1} , and when solving for N_{Er} , we estimated a value of 2.7×10^{20} cm^{-3} .

The excitable Er^{3+} density we found from Fig. 11 is rather consistent with the amount measured by RBS (see Table I); so, the conclusion is straightforward: most of the Er is optically active in the samples but only a tiny percentage of it can be excited through the Si-nc. This observation strongly supports our previous suggestions of assigning the signal enhancement obtained under resonant pumping conditions ($\sim 6 \times 10^{21}$ $\text{cm}^{-2} \text{s}^{-1}$ at 488 nm) to a dominant direct excitation of Er.²⁰

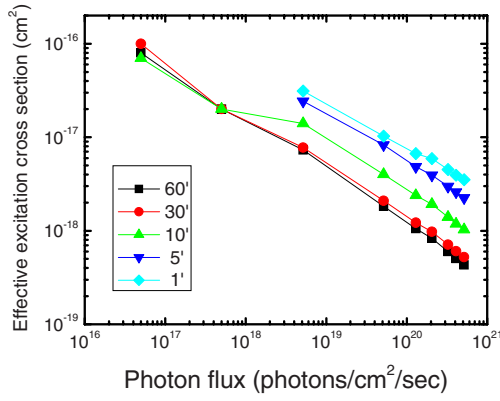


FIG. 12. (Color online) Effective excitation cross section as a function of pumping flux of photons at 476 nm for all the samples studied in this work; the legend refers to the annealing time.

2. Experimental evidences of a distance-dependent interaction

In a recent paper we have demonstrated that the low fraction of potentially excitable Er through the Si-nc can be explained by assuming that the energy transfer between Si-nc and Er ions is strongly dependent on their mutual distance.²⁵ Our paper introduced a distance-dependent interaction model that we will develop in detail in the following sections, together with experimental evidences of such a distance-dependent interaction. In Eq. (10) we have previously defined the effective excitation cross section σ_{eff} , which actually is the rate allowing a given pumping relay to excite Er. Thus, the lower is the σ_{eff} , the more difficult it is to excite further Er ions; σ_{eff} is of about 10^{-16} cm² at a low flux of $\sim 10^{16}$ cm⁻² s⁻¹ (see above), so as to say a large cross section comparable to that of the Si-nc. So, it means that the first pumped Er ions are excited at a very high rate and efficiently from the pump; from the calculations above for the sample annealed at 60' we are able to estimate that only about $\sim 5 \times 10^{16}$ Er ions benefit from that high cross section. These privileged Er ions are located on the appropriate location with regards to the excitation of the Si-nc, probably in the transition region between the Si-nc and the matrix.³⁴ Those privileged Er ions emit and are thus observable in routine PL experiments at low pumping flux. From such observations, it was assumed that all Er present in the sample would show similar behavior, allowing the use of Si-nc+Er materials as a high gain medium with low power pumping sources. However, even at moderate pumping fluxes of 5×10^{18} cm⁻² s⁻¹, i.e., those of a high power LED, the σ_{eff} has decreased to the 10^{-18} cm² order of magnitude (60' sample, see Table II) and the amount of Er excited is only $\approx 2 \times 10^{18}$ cm⁻³, which is roughly 1 over 200 ions.

From Eq. (10), we can calculate σ_{eff} for higher fluxes without making any assumption on the mechanism by which Er is pumped. Figure 12 represents σ_{eff} for all samples as a function of flux over the five decades of fluxes range. It is worth remarking that σ_{eff} has been calculated in this work by considering only the Er coupled to the Si-nc ($N_{2 \text{ max}}$ in Fig. 6 and Table II). The obtained values reflect, therefore, some averaging of the pumping efficiency among the whole indi-

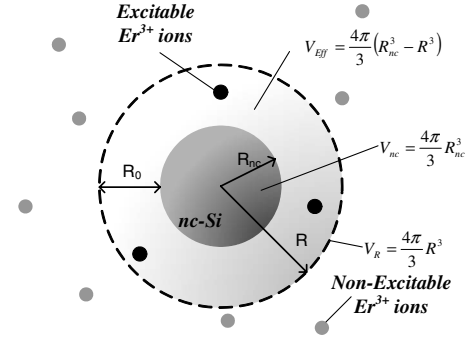


FIG. 13. Schematic explanation for Eqs. (17) and (18). Only Er³⁺ ions within interaction radius R can be excited via energy transfer from Si-nc (black circles) and Er³⁺ ions outside of interaction sphere with a volume of $\frac{4\pi R^3}{3}$ are hindered from the excitation (gray circles).

rectly excitable Er ions (but not all existing Er as in Ref. 25).

The trends of Fig. 12 are clear hints of a distance-dependent interaction. First of all, all the curves show the significant decrease of σ_{eff} with increasing pumping flux, i.e., when additional Er is excited. In fact, σ_{eff} as defined in Eq. (10) is the result of the energy transfer from excited Si-nc (N_{Si}^*). Excited Si-nc pump Er ions at a rate $K_1 N_{\text{Si}}^* N_1$, so they are related by

$$\sigma_{\text{eff}} = K_1 \frac{N_{\text{Si}}^*}{\varphi}. \quad (16)$$

Since N_{Si}^* is expected to linearly increase with φ at low or moderate pump flux, Eq. (16) is clearly illustrating that, as seen in Fig. 12, the dependence of σ_{eff} on φ is mainly attributed to the pump flux-dependent K_1 . While other quenching mechanisms failed to explain the low amount of excitable Er, the results of Fig. 12 thus indicate that the coupling constant between Si-nc and Er (K_1) should rapidly drop with the increasing flux, as both are intimately related.

Additional Er ions involved might imply their location at a longer distance from the sensitizer (Si-nc). Then if we assume that each Si-nc transfers its excitation to the closest unexcited Er ions, it is possible to define an effective volume V_{eff} around each Si-nc that contains the excited Er ions. Thus, the density of Er ions in such V_{eff} is the product of the total volume of V_{eff} and the density of Er ions in the film, as

$$N_2 = N_{\text{Si}} V_{\text{eff}} N_{\text{Er}}. \quad (17)$$

V_{eff} can be evaluated as the subtraction of the volume of Si-nc from the interaction sphere with interaction radius R as

$$R = \left[\left(\frac{3}{4\pi} \frac{N_2}{N_{\text{Si}} N_{\text{Er}}} \right) + R_{\text{nc}}^3 \right]^{1/3}. \quad (18)$$

Figure 13 schematically explains the calculation of R . The average radius R_{nc} of the Si-nc has been determined from EFTEM measurements and the value obtained is 1.6 nm. The measurement of the concentration of Si-nc has been considered in the experimental section as was found to be $\sim 3 \times 10^{17}$ cm⁻³. However, for the purpose of this section it is enough to calculate the volume occupied by the absolute

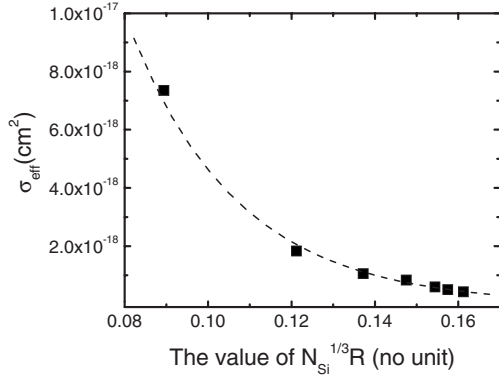


FIG. 14. Exponential dependence of the effective excitation cross section as a function of the interaction radius.

number N_2 and then translate $\sigma_{\text{eff}}(\varphi)$ into $\sigma_{\text{eff}}(N_{\text{Si}}^{1/3}R)$. The result is shown in Fig. 14 and displays a clear exponential dependence; the fit of the experimental data to an exponential decay $\sigma_{\text{eff}} = \sigma_0 \exp(-N_{\text{Si}}^{1/3}R/\rho)$ results in $\sigma_0 = 4.36 \times 10^{-16} \text{ cm}^2$ and $\rho = 0.0217$. One can get also an estimate of N_{Si} by assuming that for the lowest flux used in this experiment, the few Er ions excited are very close to the surface of the Si-nc. Thus, the value estimated is $N_{\text{Si}} \approx 1.7 \times 10^{17} \text{ cm}^{-3}$, quite close to the experimental value obtained by EFTEM. Using this value and the fitting parameter ρ , we can also estimate a characteristic interaction length between the Si-nc and the Er that is $R_0 \approx 0.4 \text{ nm}$. This distance-dependent interaction has been also suggested earlier in the literature with similar R_0 values.^{35,36}

V. MODELING AND DISCUSSION

Starting from the Si-nc and the Er^{3+} ions rate equations (1) and (2), and using the above reported results, we develop the rate equations describing the distance-dependent interaction between Si-nc and Er. The main objective is to determine the maximum amount of Er ions that can be excited through the Si-nc once the concentration of exciting clusters is known. To achieve this, we have built up a computer code in which we have modeled the Si-nc as a quasi-two-level system and considered a multilevel scheme for the Er ions. However, for the sake of a better physical insight, hereafter we work out in detail an analytical simplified version of the coupled rate equations in which Er ions are taken as a quasi-two-level system. The refinement provided by the five-levels scheme is marginal and in the following we shall mention only the analytical approach.

The simplified coupled equations are basically the same as those developed and justified above using Eqs. (1) and (2), but include some modifications: (i) ESA and AEE are neglected, (ii) CUC is considered by introducing $\tau_{\text{PL}}(\varphi)$ of Eq. (13), and (iii) the excitation coefficient K_1 is assumed dependent on the distance between the Si-nc and Er^{3+} ion. As a result, the set of rate equation for the Si-nc subsystem and Er^{3+} ion in the coupled system can be simplified from Eqs. (1) and (2) as

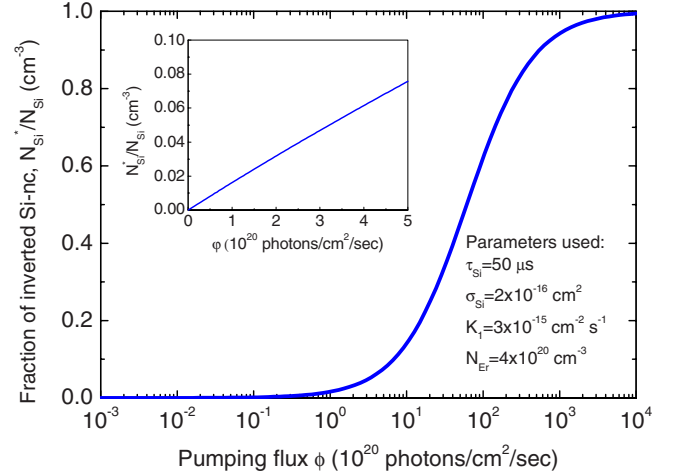


FIG. 15. (Color online) Fraction of excited Si-nc as a function of photon flux in the range 10^{17} – 10^{24} photons/cm² s. The inset shows in linear scale the range up to 5×10^{20} photons/cm² s to illustrate the linear dependence of excited Si-nc up to this high photon flux.

$$\frac{dN_{\text{Si}}^*}{dt} = \sigma_{\text{Si}} N_{\text{Si}}^0 \varphi - \frac{N_{\text{Si}}^*}{\tau_{\text{Si}}} - K_1 N_{\text{Si}}^* N_1,$$

$$\frac{dN_2}{dt} = K_1 N_{\text{Si}}^* N_1 - \frac{N_2}{\tau_{\text{PL}}(\varphi)}. \quad (19)$$

The excitation cross sections of Si-nc and Er, lifetimes of Er in the first excited state, CUC coefficients, and Er and Si-nc concentrations have been measured for our materials and the results were described in the previous experimental sections. For the other parameters we have used the values reported in the literature.^{14,15,17,19}

In steady-state pumping conditions, the time derivatives are zero and the density of excited Si-nc is

$$N_{\text{Si}}^* = \frac{N_{\text{Si}} \varphi}{\varphi + \frac{1}{\sigma_{\text{Si}} \tau_{\text{Si}}} + \frac{K_1 N_1}{\sigma_{\text{Si}}}}. \quad (20)$$

Since $\sigma_{\text{eff}} \varphi = K_1 N_{\text{Si}}^*$, we noted in previous sections that σ_{eff} gets flux dependent as soon as N_{Si}^* departs from the linear dependence versus flux, even by considering K_1 as a constant, independent of the interaction distance. This is clearly due to the fact that Er excitation comes from the transfer of a two-level system that can be saturated, and not directly from the pumping photons. Figure 15 illustrates the dependence of N_{Si}^* versus the pumping flux over a wide range of 10^{17} – 10^{24} photons/cm² s. As shown in the inset in linear scale, departure from linearity starts well above $5 \times 10^{20} \text{ cm}^{-2} \text{ s}^{-1}$, the maximum experimental flux used in this work for nonresonant excitation. This clearly demonstrates that the progressive drop in σ_{eff} with increasing pump is not due to the saturation of absorbers (Si-nc), and therefore its definition is meaningful.

By solving Eq. (19) in steady state, the fraction of Er in the first excited state becomes

$$\frac{N_2}{N_{\text{Er}}} = \frac{1}{1 + \frac{1}{\tau_{\text{PL}} K_1 N_{\text{Si}}}}. \quad (21)$$

At this point one can insert the excited population of Si-nc given by Eq. (20) into Eq. (21) and rearrange all the terms to get the typical sigmoidal curve of a two-level system. Similarly to Eq. (6), by expressing the sigmoid (18) in the standard way, he gets to

$$\frac{N_2}{N_{\text{Er}}} \approx \frac{\varphi}{\varphi + 1/\sigma_{\text{eff}}\tau_{\text{PL}}} \equiv \alpha \left(\frac{\varphi}{\varphi + 1/\sigma_{\text{eff}}^*\tau_{\text{PL}}} \right). \quad (22)$$

This expression owns a proportionality factor (α), that results from the fact that excitation of Er is an indirect process. Therefore the pumping is limited by the saturation of absorbers (Si-nc) and competes with the intrinsic deexcitation of Er. This allows one to define the maximum excitable Er fraction (α), and redefine the effective excitation cross section σ_{eff}^* that replaces σ_{eff} for the coupled system as follows:

$$\alpha = \frac{K_1 N_{\text{Si}}}{\frac{1}{\tau_{\text{PL}}} + K_1 N_{\text{Si}}}, \quad (23)$$

$$\sigma_{\text{eff}}^* = \sigma_{\text{Si}} \left(\frac{\frac{1}{\tau_{\text{PL}}} + K_1 N_{\text{Si}}}{\frac{1}{\tau_{\text{Si}}} + K_1 N_1} \right). \quad (24)$$

Equation (24) enlightens that in a regime of low pumping flux, where transfer dominates over intrinsic deexcitations, $\sigma_{\text{eff}}^* \sim \sigma_{\text{Si}} N_{\text{Si}} / N_{\text{Er}}$ and thus it scales with the density ratio between Si-nc and Er. Consequently, it is convenient to equalize both concentrations to take full advantage of the large cross section of Si-nc. The coefficient α is just the maximum amount of Er ions that can be inverted, i.e., the balance between the maximum possible pumping from Si-nc (all Si-nc excited) and the Er deexcitation as follows:

$$\alpha = \lim_{\varphi \rightarrow \infty} \frac{N_2}{N_{\text{Er}}}. \quad (25)$$

This implies a fraction $(1 - \alpha)N_{\text{Er}}$ that will never be inverted. These latter expressions depend on the energy transfer coefficient K_1 and thus will depend on the way K_1 varies with pumping flux and interaction distance. Results in Sec. IV C and Fig. 14 have revealed that the transfer term K_1 can be described as a decreasing exponential with an estimated characteristic distance $R_0 \approx 0.4$ nm, so that we postulate

$$K_1(R) = K_0 e^{-(R - R_{\text{nc}})/R_0}, \quad (26)$$

where R_{nc} is the radius of the Si-nc and K_0 is the energy transfer coefficient for low fluxes, i.e., when the transfer occurs for the Er ions that are the closest to the Si-nc. We take for this coefficient the literature value $K_0 = 3 \times 10^{-15} \text{ cm}^3 \text{ s}^{-1}$ calculated from the measurement of transfer times $\leq 1 \mu\text{s}$.¹⁵ Then, for the closest Er ions ($R = R_{\text{nc}}$) and by taking $N_{\text{Si}} \approx 3 \times 10^{17} \text{ cm}^{-3}$, $K_0 N_{\text{Si}} \approx 1 \times 10^3 \text{ s}^{-1}$ and compar-

ing with $\tau_{\text{Er}}^{-1} \approx 200 \text{ s}^{-1}$, one can observe that even if the whole Er population were coupled with that coefficient, the Si-nc would be able to pump a maximum of 83% of the Er ions. As K_1 quickly drops with increasing the relative distance, $\alpha(R)$ will drop as well and will tend to zero after few interaction lengths. Thus, by looking at Eqs. (23) and (26), it is apparent that both the density of Si-nc (N_{Si}) and the characteristic length of the interaction (R_0) are the crucial parameters that rule the amount of excitable Er.

Let us express in Eq. (19) the dependence of the parameters with interaction distance (see Fig. 13 for a schematic view) as follows:

$$\frac{N_2}{N_{\text{Er}}} = f(\varphi, R) = \frac{\alpha(R)\varphi}{\varphi + \frac{1}{\sigma_{\text{eff}}^*(R)\tau_{\text{PL}}}}. \quad (27)$$

Then, the total population N_2 as a function of flux can be calculated by spatial integration of Eq. (23) over the volume of influence of each Si-nc ($N_{\text{Si}}^{-1} \text{ cm}^3$) as follows:

$$f(\varphi) = 4\pi N_{\text{Si}} \int_{R_{\text{nc}}}^{R_{\text{max}}} f(\varphi, R) R^2 dR. \quad (28)$$

By integrating $\alpha(R)$ one obtains the maximum fraction of excitable Er as follows:

$$\alpha = 4\pi N_{\text{Si}} \int_{R_{\text{nc}}}^{R_{\text{max}}} \frac{R^2 dR}{1 + \frac{1}{K_0 N_{\text{Si}} \tau_{\text{PL}}} e^{(R - R_{\text{nc}})/R_0}}. \quad (29)$$

This integral cannot be analytically resolved and it resembles the Fermi-Dirac integrals in statistics. All the parameters inside the integral have been measured and discussed before. The density of Si-nc is about $3 \times 10^{17} \text{ cm}^{-3}$ although, by taking into account the large error bars of the EFTEM measurements and the fact that tiny Si-nc can escape observation, we will let N_{Si} vary around this value and present all the results as a function of N_{Si} .

In order to set up an upper limit for the Er excited we carry out the calculations for the best performing sample, the one annealed for 1 h. All the other samples show a much lower τ_{PL} and their excitable Er fraction scales accordingly. After numerically calculating the integral, we found $\alpha \approx 1.23\%$ for $N_{\text{Si}} \approx 3 \times 10^{17} \text{ cm}^{-3}$, quite close to the experimental value of 1.76%. In Fig. 16 the maximum excitable Er fraction is depicted as a function of the Si-nc density. By letting N_{Si} vary from 1×10^{17} to $1 \times 10^{18} \text{ cm}^{-3}$ one finds that α moves from 0.2 up to 7.8%, still a value clearly unsatisfactory. In order to get a high α value, useful to reach optical gain, such as, for instance 75%, N_{Si} should increase up to $2 \times 10^{19} \text{ cm}^{-3}$. This density value, for the range of Si excess used in this work, means that Si clusters should not include more than 175 atoms, which is equivalent to a diameter of about 1.6 nm (average size in this work is 3.2 nm).

Whether it is possible or not to engineer a material with such high density of very small clusters is just mere speculation. In principle, cluster nucleation density depends on the deposition method (clusters are already present in the as-deposited material) and on the postprocessing annealing step.

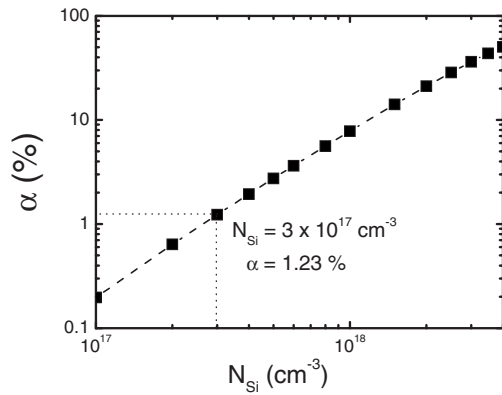


FIG. 16. Excitable Er fraction as a function of the concentration of sensitizers (Si nanoclusters) calculated from the distance-dependent interaction model developed in this work. The input parameters of the simulation correspond to the sample annealed at 60'.

Among several Si-nc thin film fabrication methods, film deposition at high temperature promotes Si diffusion and clustering during film growth and is thus not desirable for smaller clusters. SiO_x materials deposited at low temperature with defects such as voids and H impurities can provide a large number of nucleation centers. Such deposition methods, combined with flash lamp annealing or rapid thermal processes could succeed in forming small clusters with the desired diameter. Nevertheless, it is under question if such a hypothetical large amount of small clusters would still have the large excitation cross section that is the most important and distinctive feature of large clusters.

VI. CONCLUSIONS

Detailed investigations have been performed on Er-doped silicon-rich silicon oxide thin films to determine their feasibility as a gain material for optical amplifiers. Once demonstrated that the emission cross section of Er is of the same order as that in pure silica, i.e., $\sim 10^{-21}$ cm², the only advantage of introducing Si-nc is the high absorption cross section ($\sim 10^{-16}$ cm²) and the broad absorption in visible range. The studies have been done for materials with optimum Si excess (7%) and Er concentration (4×10^{20} cm⁻³) annealed different

durations. A density of clusters of about 3×10^{17} cm⁻³ and an average size of 3.2 nm was obtained from EFTEM measurements. Er effective excitation cross section is comparable to that of Si-nc only for very small pumping flux ($\sim 10^{16}$ cm⁻² s⁻¹), it drops roughly one order of magnitude per decade of increasing flux. The quantification of the light emission of the samples has allowed one to determine a maximum of excitable Er around the 2% at high pumping photon flux ($\sim 10^{21}$ cm⁻² s⁻¹), implying that only a tiny fraction of all the Er is thus coupled to the Si-nc. The effect of deexcitation phenomena that cause depletion of Er inversion such as cooperative up conversion, excited-state absorption, and Auger deexcitations has been quantified. Their impact on Er inversion would be significant only if a high fraction of Er could be inverted, while it is marginal for the materials studied here.

Instead, Auger-type short-range energy transfer from Si-nc to Er with a characteristic interaction distance of ~ 0.4 was found. Then a model based on the rate equations has been developed for the interaction of Si-nc with Er, which is dependent on the mutual distance taking into account an energy transfer process whose strength exponentially decreases with the distance. The model predicts that the transfer is quenched for high photon fluxes and that only 1–2 % of Er emitters is excitable in our materials. A low Si-nc density and the short-range character of the energy transfer imply that a significant fraction of the Er ions is out of reach by Si-nc. According to the simulation, in order to obtain a large fraction of Er ions coupled as high as 75%, Si-nc density should increase to $\sim 10^{19}$ cm⁻³. This density value, for the range of Si excess used in this work, means that Si-nc should have an average diameter of about 1.6 nm. Therefore we conclude that the main limitation to obtain gain in such a system is the low density of sensitizers and the short range of the interaction.

ACKNOWLEDGMENTS

This work has been partially supported by EU through IST LANCER project and by the Spanish Ministry of Education through the MILES-SILUZ project. The authors wish to thank Josep Carreras for writing of the MATLAB code and Olivier Jambois and Youcef Lebour for useful discussions.

¹E. Desurvive, J. R. Simpson, and P. C. Becker, *Opt. Lett.* **12**, 888 (1987).

²W. J. Miniscalco, *J. Lightwave Technol.* **9**, 234 (1991).

³A. Kévorkian, in *Fiber Optic Communication Devices*, edited by N. Grote and H. Venghaus (Springer-Verlag, Berlin, 2001), Chap. 6.

⁴A. J. Kenyon, P. F. Trwoga, M. Federighi, and C. W. Pitt, *J. Phys.: Condens. Matter* **6**, L319 (1994).

⁵T. Shimizu-Iwayama, K. Fujita, S. Nakao, K. Saitoh, T. Fujita, and N. Itoh, *J. Appl. Phys.* **75**, 7779 (1994).

⁶Y. Kanemitsu, T. Ogawa, K. Shiraishi, and K. Takeda, *Phys. Rev.*

B **48**, 4883 (1993).

⁷K. S. Min, K. V. Shcheglov, C. M. Yang, H. A. Atwater, M. L. Brongersma, and A. Polman, *Appl. Phys. Lett.* **69**, 2033 (1996).

⁸B. Garrido, M. López, O. González, A. Pérez-Rodríguez, J. R. Morante, and C. Bonafos, *Appl. Phys. Lett.* **77**, 3143 (2000).

⁹M. Perálvarez, C. García, M. López, B. Garrido, J. Barreto, C. Domínguez, and J. A. Rodríguez, *Appl. Phys. Lett.* **89**, 051112 (2006).

¹⁰M. V. Wölkín, J. Jorne, P. M. Fauchet, G. Allan, and C. Delerue, *Phys. Rev. Lett.* **82**, 197 (1999).

¹¹S. Tiwari, *Appl. Phys. Lett.* **68**, 1377 (1996).

- ¹²O. González-Varona, B. Garrido, S. Cheylan, A. Pérez-Rodríguez, A. Cuadras, and J. R. Morante, *Appl. Phys. Lett.* **82**, 2151 (2003).
- ¹³G. Franzó, S. Bonitelli, D. Pacifici, F. Priolo, F. Iacona, and C. Bongiorno, *Appl. Phys. Lett.* **82**, 3871 (2003).
- ¹⁴P. G. Kik, M. L. Brongersma, and A. Polman, *Appl. Phys. Lett.* **76**, 2325 (2000).
- ¹⁵D. Pacifici, G. Franzó, F. Priolo, F. Iacona, and L. Dal Negro, *Phys. Rev. B* **67**, 245301 (2003).
- ¹⁶H. S. Han, S. Y. Seo, J. H. Shin, and D. S. Kim, *J. Appl. Phys.* **88**, 2160 (2000).
- ¹⁷E. Snoecks, G. N. van den Hoven, and A. Polman, *IEEE J. Quantum Electron.* **32**, 1680 (1996).
- ¹⁸H. S. Han, S. Y. Seo, and J. H. Shin, *Appl. Phys. Lett.* **79**, 4568 (2001).
- ¹⁹J. H. Shin, J. Lee, H. S. Han, J. H. Jhe, J. S. Chang, S. Y. Seo, H. Lee, and N. Park, *IEEE J. Sel. Top. Quantum Electron.* **12**, 783 (2006).
- ²⁰N. Daldosso, D. Navarro-Urrios, M. Melchiorri, L. Pavesi, F. Gourbilleau, M. Carrada, R. Rizk, C. Garcia, P. Pellegrino, B. Garrido, and L. Gognolato, *Appl. Phys. Lett.* **86**, 261103 (2005); **88**, 161901 (2006).
- ²¹H. Mertens, A. Polman, I. M. P. Aarts, W. M. M. Kessels, and M. C. M. van den Sanden, *Appl. Phys. Lett.* **86**, 241109 (2005).
- ²²P. Pellegrino, B. Garrido, J. Arbiol, C. Garcia, Y. Lebour, and J. R. Morante, *Appl. Phys. Lett.* **88**, 121915 (2006).
- ²³C. Garcia, B. Garrido, P. Pellegrino, R. Ferré, J. A. Moreno, J. R. Morante, L. Pavesi, and M. Cazzanelli, *Appl. Phys. Lett.* **82**, 1595 (2003).
- ²⁴C. J. Oton, W. H. Loh, and A. J. Kenyon, *Appl. Phys. Lett.* **89**, 031116 (2006).
- ²⁵B. Garrido, C. García, P. Pellegrino, D. Navarro-Urrios, N. Daldosso, L. Pavesi, F. Gourbilleau, and R. Rizk, *Appl. Phys. Lett.* **89**, 163103 (2006).
- ²⁶F. Gourbilleau, L. Levalois, C. Dufour, J. Vicens, and R. Rizk, *J. Appl. Phys.* **95**, 3717 (2004).
- ²⁷N. Daldosso, D. Navarro-Urrios, M. Melchiorri, C. Garcia, P. Pellegrino, B. Garrido, C. Sada, G. Battaglin, F. Gourbilleau, R. Rizk, and L. Pavesi, *IEEE J. Sel. Top. Quantum Electron.* **12**, 1607 (2006).
- ²⁸F. Iacona, C. Bongiorno, C. Spinella, S. Boninelli, and F. Priolo, *J. Appl. Phys.* **95**, 3723 (2004).
- ²⁹I. Izeddin, A. S. Moskalenko, I. N. Yassievich, M. Fujii, and T. Gregorkiewicz, *Phys. Rev. Lett.* **97**, 207401 (2006).
- ³⁰K. Watanabe, M. Fujii, and S. Hayashi, *J. Appl. Phys.* **90**, 4761 (2001).
- ³¹J. Palm, F. Gan, B. Zheng, J. Michel, and L. C. Kimerling, *Phys. Rev. B* **54**, 17603 (1996).
- ³²S.-Y. Seo and J. H. Shin, *Appl. Phys. Lett.* **75**, 4070 (1999).
- ³³K. Imakita, M. Fujii, Y. Yamaguchi, and S. Hayashi, *Phys. Rev. B* **71**, 115440 (2005).
- ³⁴N. Daldosso, M. Luppi, S. Ossicini, E. Degoli, R. Magri, G. Dalba, P. Fornasini, R. Grisenti, F. Rocca, L. Pavesi, S. Boninelli, F. Priolo, C. Spinella, and F. Iacona, *Phys. Rev. B* **68**, 085327 (2003).
- ³⁵J. H. Jhe, J. H. Shin, K. J. Kim, and D. W. Moon, *Appl. Phys. Lett.* **82**, 4489 (2003).
- ³⁶F. Gourbilleau, R. Madelon, C. Dufour, and R. Rizk, *Opt. Mater. (Amsterdam, Neth.)* **27**, 868 (2005).